

Taklimakan dust aerosol radiative heating derived from CALIPSO observations using the Fu-Liou radiation model with CERES constraints

J. Huang¹, Q. Fu^{2,1}, J. Su¹, Q. Tang¹, P. Minnis³, Y. Hu³, Y. Yi⁴, and Q. Zhao⁵

¹Key Laboratory for Semi-Arid Climate Change of the Ministry of Education, College of Atmospheric Sciences, Lanzhou University, Lanzhou, 730000, China

²Department of Atmosphere Science, University of Washington, USA

³NASA Langley Research Center, Hampton, VA, 23666, USA

⁴Science Systems and Applications Inc., Hampton, VA 23666, USA

⁵Gansu Meteorological Bureau, Lanzhou, 73000 China

Received: 25 November 2008 – Published in Atmos. Chem. Phys. Discuss.: 5 March 2009

Revised: 5 May 2009 – Accepted: 29 May 2009 – Published: 18 June 2009

Abstract. The dust aerosol radiative forcing and heating rate over the Taklimakan Desert in Northwestern China in July 2006 are estimated using the Fu-Liou radiative transfer model along with satellite observations. The vertical distributions of the dust aerosol extinction coefficient are derived from the CALIPSO (Cloud-Aerosol Lidar and Infrared Pathfinder Satellite Observations) lidar measurements. The CERES (Cloud and the Earth's Energy Budget Scanner) measurements of reflected solar radiation are used to constrain the dust aerosol type in the radiative transfer model, which determines the dust aerosol single-scattering albedo and asymmetry factor as well as the aerosol optical properties' spectral dependencies. We find that the dust aerosols have a significant impact on the radiative energy budget over the Taklimakan desert. In the atmospheres containing light, moderate and heavy dust layers, the dust aerosols heat the atmosphere (daily mean) by up to 1, 2, and 3 K day⁻¹, respectively. The maximum daily mean radiative heating rate reaches 5.5 K day⁻¹ at 5 km on 29 July. The averaged daily mean net radiative effect of the dust are 44.4, -41.9, and 86.3 W m⁻², respectively, at the top of the atmosphere (TOA), surface, and in the atmosphere. Among these effects about two thirds of the warming effect at the TOA is related to the longwave radiation, while about 90% of the atmospheric warming is contributed by the solar radiation. At the surface, about one third of the dust solar radiative

cooling effect is compensated by its longwave warming effect. The large modifications of radiative energy budget by the dust aerosols over Taklimakan Desert should have important implications for the atmospheric circulation and regional climate, topics for future investigations.

1 Introduction

Aerosols influence the radiative energy budget directly by scattering and absorbing solar radiation (*direct effect*), and indirectly by altering cloud droplet size distribution and concentration (*Indirect effect*) (Twomey, 1977; Albrecht, 1989). Absorbing aerosols, such as black carbon and mineral dust, could contribute to large diabatic heating in the atmosphere that often enhances cloud evaporation (*semi-indirect effect*) (Ackerman et al., 2000; Koren et al., 2004; Kruger and Graßl, 2004; Huang et al., 2006). The magnitude of the global mean radiative effect of dust aerosols is comparable to that of anthropogenic aerosols from sulphates and biomass combustion (Sokolik and Toon, 1999). Dust aerosols also have a significant greenhouse effect through longwave radiation which warms both the surface and atmosphere (e.g., Zhang and Christopher 2003). However, there are considerable uncertainties in estimating the radiative effects of dust aerosols. The net radiative effect at the top-of-atmosphere (TOA) could be either positive or negative, depending on several key variables, such as surface albedo, particle size, vertical distribution of the dust layer, dust optical depth, and



Correspondence to: J. Huang
(hjp@lzu.edu.cn)

the imaginary part of the refractive index (Liao and Seinfeld, 1998). Recently, Satheesh et al. (2006) studied the atmospheric warming due to dust aerosols over the Afro-Asian region. They found a reduction of solar radiation reaching at the surface with a lower atmospheric warming of 0.3 to 0.5 K day⁻¹.

The vertical distribution of dust aerosols is one of the critical parameters in the assessment of the dust radiative effect (Claquin et al., 1998; Zhu et al., 2007). A model study by Carlson and Benjamin (1980) showed that an elevated Saharan dust layer could change the atmospheric heating rate dramatically. Liao and Seinfeld (1998) claimed that clear sky long-wave radiative forcing and cloudy sky TOA shortwave (SW) radiative forcing of dust aerosols are very sensitive to the altitude of the dust and cloud layers. Meloni et al. (2005) also found that SW aerosol radiative forcing at the TOA has a significant dependence on aerosol vertical profiles.

The recently launched CALIPSO satellite provides a wealth of actively sensed vertical structures of aerosols over regional and global scales and provides an unprecedented opportunity to study the radiative effects of dust aerosols. Unlike the space-based passive remote sensing instruments, CALIPSO can observe aerosols over bright surfaces and beneath thin clouds as well as in clear sky conditions (Winker et al., 2006; Hu et al., 2006, 2007; Liu et al., 2004, 2008; Huang et al., 2007, 2008). One of the most distinct advantages of the CALIPSO lidar observations is that it provides a direct measure of the vertical structure of aerosols.

This paper estimates the dust aerosol radiative heating rate and the radiative effect during the dust events that occurred over the Taklimakan Desert in the summer of 2006. The Taklimakan Desert is a significant source of airborne dust that affects much of Eastern Asia, the Northern Pacific, and sometimes North America (references, Huang et al., 2008). The Fu-Liou radiation model (Fu and Liou, 1992, 1993) is used to compute the aerosol heating rates and radiative forcing. The vertical distributions of dust aerosol extinction coefficients used in the computations are derived from the CALIPSO lidar observations. We use the reflected solar radiation measured at the top of the atmosphere (TOA) from the Clouds and Earth's Radiant Energy System (CERES) (Wielicki et al., 1996) Single Satellite Footprint (SSF) to constrain the dust aerosol type employed in the radiation model. The combination of the radiation model with the CALIPSO and CERES observations should lead to a reliable estimate of the dust aerosol radiative effects.

The paper is organized as follows. The summer Taklimakan dust events and the dust aerosol extinction profiles from CALIPSO observations are discussed in Sects. 2 and 3, respectively. The radiation model and the CERES constraint of dust aerosol single scattering albedo and asymmetry factor are described in Sect. 4. The estimation of the Taklimakan dust aerosol radiative heating and forcing is presented in Sect. 5 and summary and conclusions are given in Sect. 6.

2 Summer Taklimakan dust events

The Taklimakan Desert is a desert in Central Asia, in the Xinjiang Uyghur Autonomous Region of China, which is known as one of the largest sandy deserts in the world. It covers an area of 270 000 km² of the Tarim Basin, which is 1000 km long and 400 km wide. The Taklimakan Desert is about 1 km above sea level, surrounded by mountains except for an opening at its northeast corner.

Most Asian dust studies have focused on the late winter and spring due to observed long-range dust transport (Iwasaka et al., 1983; Zhang et al., 1997; Murayama et al., 2001; Uno et al., 2001; Sun et al., 2001; Wang et al., 2005). Uno et al. (2008) reported the 3-dimensional structure of Asian dust outflow from a dust source region to the Northwestern Pacific Ocean. They found that the elevated dust was transported to the Pacific Ocean with the major dust layer maintaining a height between 2.5–4.0 km. There have been very few studies analyzing the specific signatures of summer and fall dust storms over the Taklimakan Desert. Recently CALIPSO lidar observations show that dust events occur throughout the year over the Taklimakan (Liu et al., 2008a) and that heavy dust storms are part of the summer weather (Huang et al., 2007). The impact of the Taklimakan dust storms on the radiative energy budget and the implication to the regional climate are open questions. In this study we will quantify the vertical structures of dust aerosol extinction coefficients and radiative effects during the dust event that occurred during the period of 26 to 31 July 2006 over the Taklimakan.

The start of the dust outbreak was associated with the intensive low pressure system over West Siberian with a trough extending from northwest toward southeast. This caused a large pressure gradient and strong northwesterly winds (>20 m/s) between 45° and 55° N, which resulted in the onset of this dust episode. During 26 July, a moderate wind and dust storm in the northern Taklimakan, accompanied by localized severe dust storms, developed and extended southward. Under the influence of this storm, a wind-blown sand and/or dust cloud persisted over northern Qinghai and Tibet through 31 July. The strong dust events mainly occurred between 27 and 29 July.

3 Vertical structures of dust aerosol extinction coefficient

CALIPSO lidar measurements are used to derive the vertical distribution of dust aerosol extinction coefficient. The CALIPSO lidar is designed to acquire vertical profiles of elastic backscatter at two wavelengths (532 and 1064 nm) from a near nadir-viewing geometry during both day and night phases of the Sun-synchronous orbit, which has a 13:30 LT equatorial crossing time. In addition to total backscatter at the two wavelengths, CALIPSO also provides

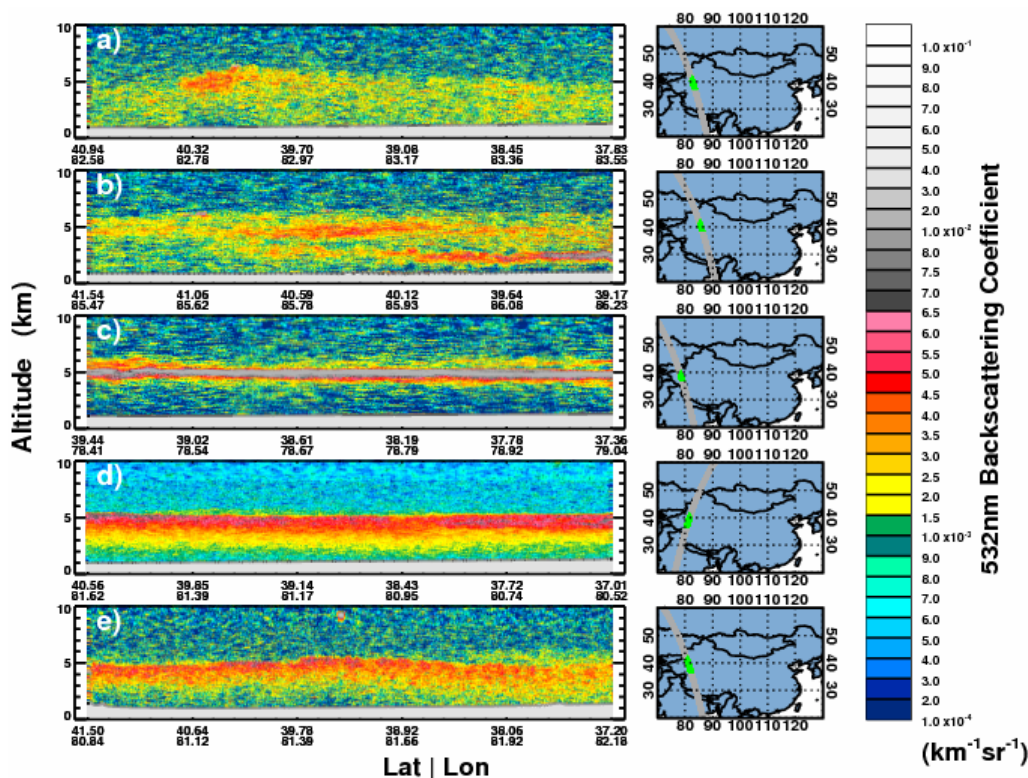


Fig. 1. The altitude-orbit cross-section of 532 nm total attenuated backscattering intensity (left panels) for the green-shaded portion of each track (right panels) over the Taklimakan Desert region (35° N–45° N) for (a) 24 July, (b) 26 July, (c) 29 July, (d) 30 July, and (e) 31 July 2006.

profiles of linear depolarization at 532 nm. The depolarization measurements enable the discrimination between ice and water clouds (Hu et al., 2007b), and the identification of non-spherical aerosol particles. The CALIPSO Level 1B data are used in this study and include a half orbit (day or night) of calibrated and geolocated single-shot lidar profiles with the highest vertical resolution. They include both 532 and 1064-nm attenuated backscatter and depolarization ratios at 532 nm. The product contains data from the nominal science mode measurement.

The dust aerosol optical depth for a given layer is retrieved in terms of backscatter from the CALIPSO lidar observations (Hu et al., 2006) in the form,

$$\tau(z) = \frac{1}{2\eta} \ln(1 - 2\gamma'(z)S_{a,\text{eff}}) \quad (1)$$

where η is the layer-effective multiple scattering factor, which is 0.7 for this study (Omar et al., 2004). $S_{a,\text{eff}}$ is the product of η and the single-scattering lidar ratio (i.e., extinction-to-backscatter ratio), which has a value of 44 here (Omar et al., 2004), and $\gamma'(z)$ is the integrated attenuated backscattering coefficient β_a from the top to the base of the layer, which is defined as

$$\gamma'(z) = \int_{z_{\text{top}}}^{z_{\text{base}}} \beta_a(z) dz \quad (2)$$

The dust aerosol extinction coefficient, β , is thus obtained from

$$\beta(z) = \frac{\tau(z)}{\Delta z} \quad (3)$$

where $\Delta z = (z_{\text{top}} - z_{\text{base}})$ is the vertical resolution, which is 30 m below and 60 m above 8.2 km, respectively.

Figure 1 shows the CALIPSO orbit-altitude cross-section of the 532-nm total attenuated backscattering coefficient from 24–31 July 2006, where daytime data were used for 24, 26, 29, and 31 July and nighttime data were taken for 30 July. The CALIPSO data reveals that vertically extended dust layers are widespread throughout the Tarim Basin with peak lidar returns between 2.5 and 5.5 km above mean sea level (MSL). In general, the red-gray-white color scales used in CALIPSO data analyses, as shown in Fig. 1, indicate clouds and green-yellow-orange color features are aerosols. However, the heavy dust layers over the source regions are often misclassified as clouds in the current data products because the dust aerosol optical properties including the color ratio (defined as the ratio of 1064 to 532 nm attenuated backscatter) and backscattering intensity are similar to clouds during heavy dust loading episodes (optical depth $> 1 \sim 2$) (Liu, et al., 2008a)]. For example, the heavy dust layer over the Taklimakan Desert on 29 July is misclassified as cloud (gray in Fig. 1c). Figure 2 shows the volume depolarization

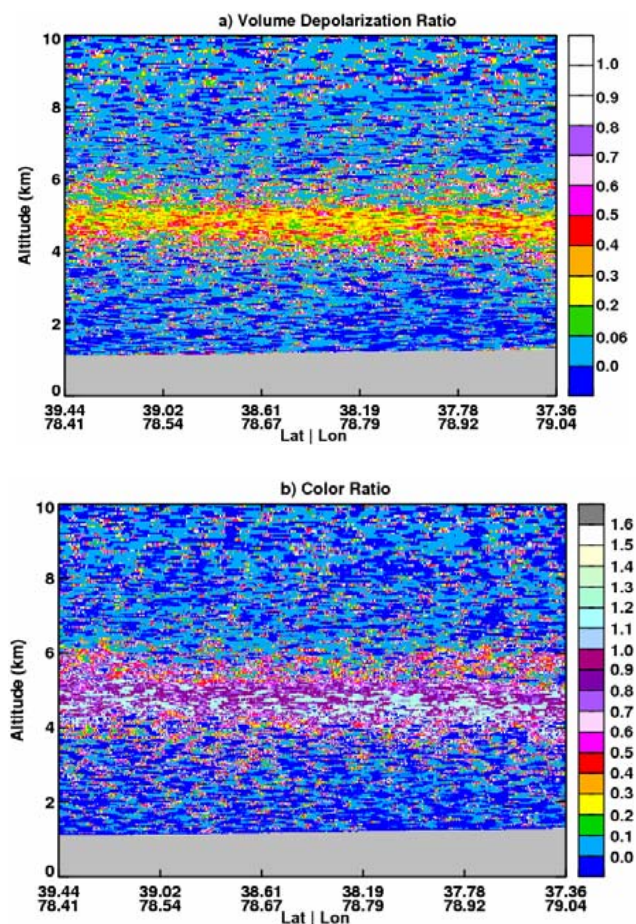


Fig. 2. The altitude-orbit cross-section of (a) volume depolarization ratio and (b) 1064-nm/532-nm backscatter color ratio for 29 July 2006 over the Taklimakan Desert region (35° N–45° N).

ratio (defined as the ratio of perpendicular-to-parallel components of received lidar signals at 532 nm) and the backscatter color ratio. The dust aerosols have a large depolarization ratio due to their nonsphericity (Fig. 2a), while they also have a large color ratio due to the relatively large size of the particles (Fig. 2b). On the other hand, the depolarization ratio is near zero for water clouds and other types of aerosols. Based on all this information from the CALIPSO measurements including the attenuated backscattering, depolarization ratio, and backscattering color ratio, we have identified the intensive backscattering layer in Fig. 1c as the dust layer. Independent observations from both *Aqua* MODIS (Fig. 3) and Cloudsat radar (figure not shown) confirm that the intensive dust layer occurred on 29 July.

The orbit-altitude cross sections (left) and orbit mean profiles (right) of the dust aerosol extinction coefficients are given in Fig. 4. For all cases, the dust layer can be distinctly identified. At the beginning of the dust episode (24 July), the extinction coefficient is $\sim 0.1 \text{ km}^{-1}$ from the surface to 5 km and then decreases with height above ~ 5 km. On 26 July, the

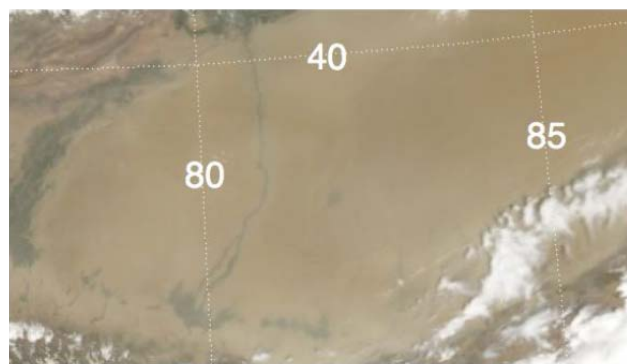


Fig. 3. The true color *Aqua* satellite image over Northwest China for 29 July 2006, in which channel $0.65 \mu\text{m}$, $0.56 \mu\text{m}$ and $0.47 \mu\text{m}$ are associated with red, green and blue colors, respectively.

elevated dust layer starts to develop as indicated by the enhanced dust aerosol extinction coefficients in Fig. 4b. From 29 to 31 July, the elevated dust layers are located at about 5 km, which leads to the transport of dust aerosols to the Tibetan plateau (Huang et al., 2007). For the heavy dust layer on 29 July (Fig. 4c), the mean dust extinction coefficient at 5 km is about 0.35 km^{-1} .

Figure 5 shows the column dust optical depth for those five days. The spatial variation of the optical depth is significant on 24 and 26 July, ranging from ~ 0.4 to 0.9 (Fig. 5a and b). On 29 and 30 July (Fig. 5c and d), the variation of dust optical depth along the CALIPSO track is small with a mean around 0.8 – 0.9 . On 31 July, the dust optical depth ranges from 0.6 to 0.8 (Fig. 5e).

4 Fu-Liou radiation model and dust aerosol type constrained with CERES measurements

We use the Fu-Liou radiation model along with the input of dust aerosol extinction coefficients from the CALIPSO observations to estimate the impact of dust aerosols on the radiative energy budget. This model was originally developed by Fu and Liou (1992, 1993) and subsequently modified by Rose and Charlock (2002) and Kato et al. (2005). It is a delta-four stream radiative transfer scheme with fifteen spectral bands from 0.175 to $4.0 \mu\text{m}$ in SW and twelve longwave (LW) spectral bands between 2850 and 0 cm^{-1} . The correlated k -distribution method is used to parameterize the non-gray gaseous absorption by H_2O , CO_2 , O_3 , N_2O and CH_4 (Fu and Liou, 1992) with the addition of CFCs and CO_2 in the window region (Kratz and Rose, 1999). The single-scattering properties of dust aerosols including normalized extinction coefficients, single-scattering albedo, and asymmetry factor are based on the four dust aerosol modes described by Hess et al. (1998). The single-scattering albedo (ω) and asymmetry factor (g) at $0.67 \mu\text{m}$ are given in Table 1 for these four dust aerosol types.

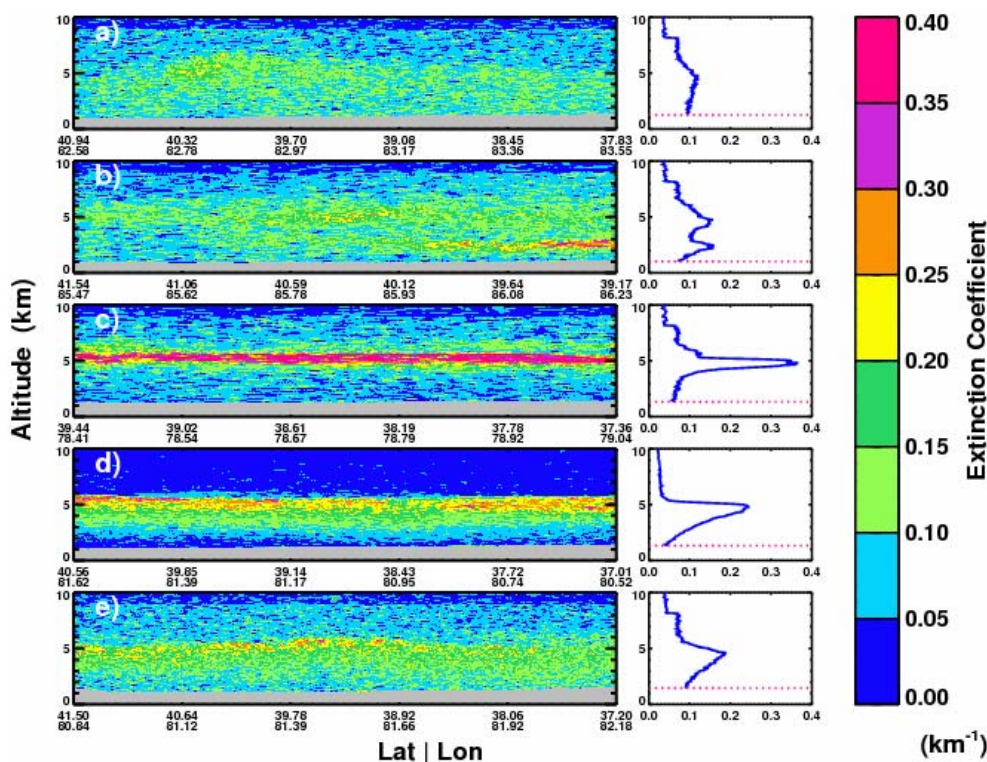


Fig. 4. The altitude-orbit cross-section of dust aerosol extinction coefficient (left panels) and orbit averaged vertical profile for (a) 24 July, (b) 26 July (c) 29 July, (d) 30 July, and (e) 31 July 2006.

Table 1. Single-scattering albedo (ω) and asymmetry factor (g) at $0.67 \mu\text{m}$ for 4 dust aerosol types used in Fu-Liou model.

	Nucleation mode	Accumulation mode	Transported mode	Coarse mode
Single-scattering albedo (ω)	0.9767	0.9203	0.89	0.7266
asymmetry factor (g)	0.6471	0.7143	0.7460	0.8613

For a given time and location, the pressure, temperature, and water vapor profiles are interpolated from the NCEP/NCAR reanalysis and ozone concentration is taken from the NCEP Stratospheric Monitoring Group Ozone Blended Analysis (SMOBA) product based on SBUV and TOVS observations. The surface albedo is based on MODIS observations as used by the CERES team (Minnis et al., 2008) with the spectral dependence prescribed for the desert scene type (T. Charlock, personal communication, 2007), which is validated with the CERES observations along the Fu-Liou radiation model. The mean value of the broadband surface albedo used in this study is 0.346 and the standard deviation is 0.005. Climatological concentrations are used for CO_2 , CH_4 , N_2O , and CFCs.

To evaluate the radiative heating and forcing due to dust aerosols, the aerosol optical properties such as extinction coefficient, single-scattering albedo and asymmetry factor are required. These properties depend upon dust characteris-

tics such as density, size distribution, and refractive index. The dust aerosol extinction coefficients at 532 nm are derived from CALIPSO measurements. In this study, we select the dust aerosol type that determines the single-scattering albedo and asymmetry factor and the spectral dependences of dust single-scattering properties by comparing the model-simulated reflected instantaneous solar radiative fluxes at the TOA with those observed by CERES. The CERES Aqua Edition 1B SSF data are used here (Wielicki et al., 1996). CERES SSF data sets combine CERES radiation measurements, MODIS cloud microphysical retrievals, and ancillary meteorology fields to form a comprehensive, high-quality compilation of satellite-derived cloud, aerosol, and radiation budget information for radiation and climate studies.

To optimize the dust aerosol single-scattering albedo and asymmetry factor used over the Taklimakan region, we compare the CERES TOA solar fluxes with Fu-Liou model simulations along the CALIPSO orbit using 4 different dust

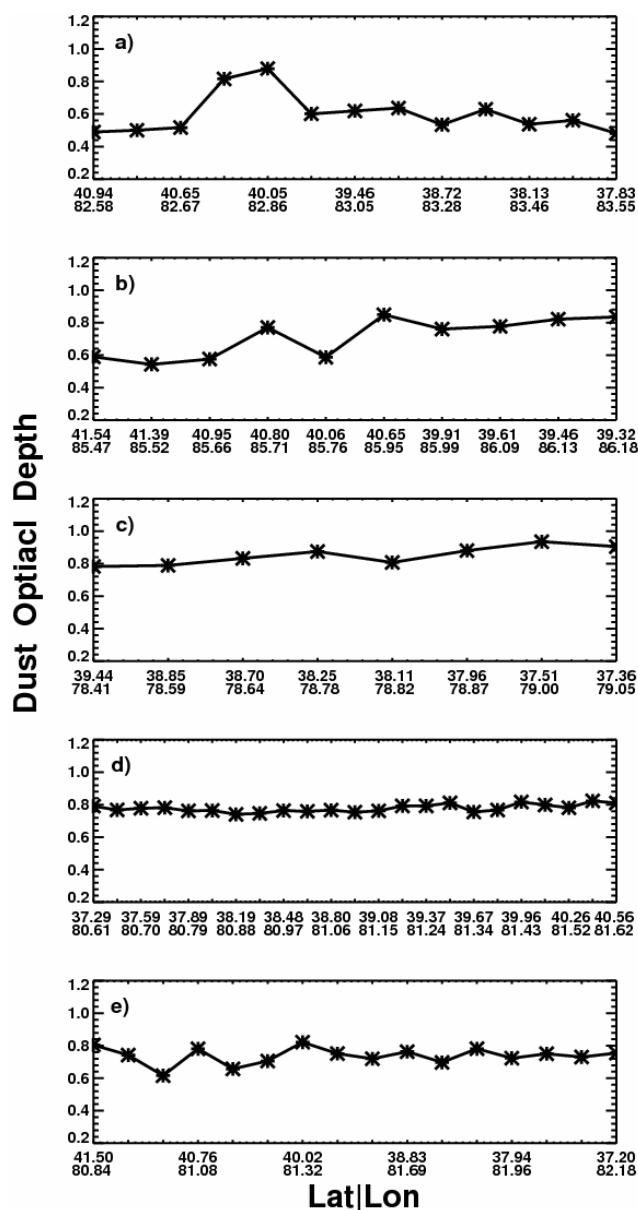


Fig. 5. Dust aerosol optical depth along CALIPSO track for (a) 24 July, (b) 26 July, (c) 29 July, (d) 30 July, and (e) 31 July 2006.

aerosol types from OPAC (Optical properties of aerosol and clouds: The software package OPAC) (Hess, et al., 1998). We found that the dust aerosol type that fits best is the transported mode. Figure 6 shows a comparison of the TOA reflected solar fluxes derived from the Fu-Liou model with CERES measurements along the CALIPSO orbit over the Taklimakan Desert region (35°N – 45°N) for the daytime cases (24, 26, 29, 31 July). The model-simulated TOA shortwave fluxes agree reasonably well with those from CERES. The averaged difference between the model simulations and CERES measurements is only 1.5 W m^{-2} . Thus, it is clear from this comparison that the radiative transfer model con-

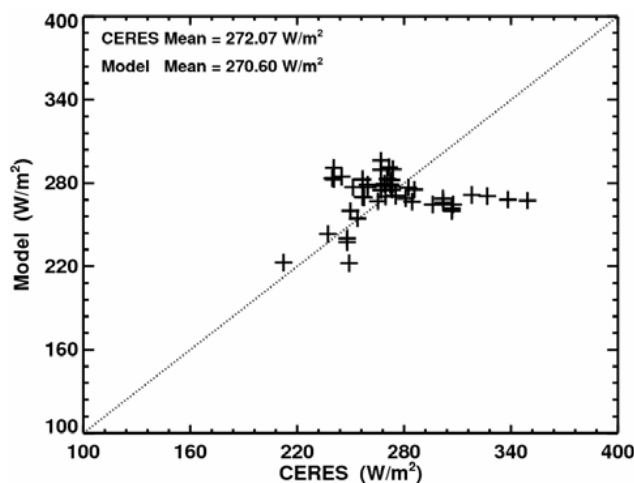


Fig. 6. Comparison of the modeled simultaneous TOA shortwave flux with CERES observations along the CALIPSO orbit over the Taklimakan Desert region (35°N – 45°N) on 24, 26, 29, and 31 July 2006.

strained with the CERES observations can be used to reliably determine the variation of dust aerosol radiative heating rates with the input of vertical distributions of dust aerosols from CALIPSO measurements.

We thus used the single-scattering albedo and asymmetry factor and their spectral dependences for the transported dust aerosol mode in all the simulations. The extinction coefficient is from

$$\beta(\lambda) = \frac{\beta(532\text{ nm})}{\beta_0(532)} \beta_0(\lambda), \quad (4)$$

where $\beta(532\text{ nm})$ is the dust extinction coefficient from CALIPSO at 532 nm and β_0 is the normalized extinction coefficients of the transported dust aerosol mode. Thus, our calculations allowed the extinction coefficient profiles to vary according to the CALIPSO observations.

5 Taklimakan dust aerosol radiative heating and forcing

Figures 7–9 show the impact of dust aerosols on the daily-mean (24 h average) SW, LW, and net heating rates, respectively. They are obtained as the differences between the simulated radiative heating rates with and without considering the observed dust aerosols. The dust has a significant effect on SW radiation. For relatively light (Fig. 7a), moderate (Fig. 7b and e) and heavy dust layers (Fig. 7c and d), dust aerosols heat the atmosphere via absorption of SW radiation by up to ~ 1 , 2, and 3 K day^{-1} , respectively. The maximum daily-mean solar radiative heating rate of 7 K day^{-1} is found at 5 km on 29 July. Figure 7 shows that the SW heating rates have a peak corresponding to the maximum dust aerosol extinction coefficient levels.

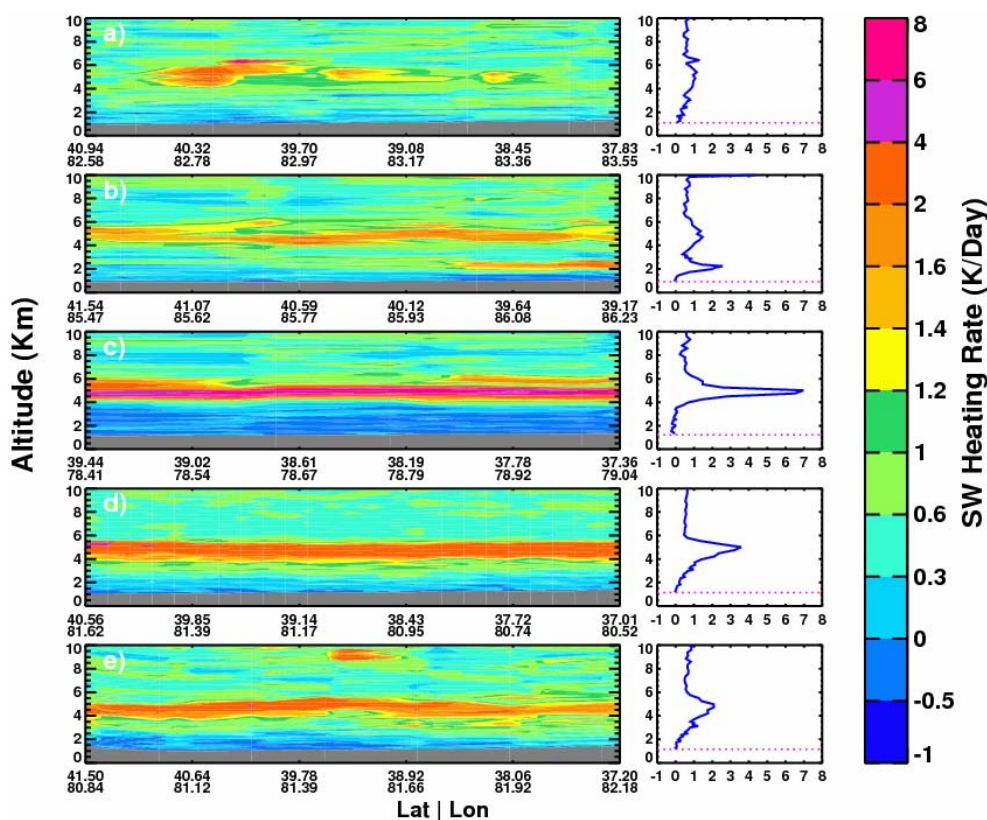


Fig. 7. The altitude-orbit cross-section of daily averaged shortwave heating rates due to dust aerosols (left panels) and the orbit-averaged vertical profile (right panels) for (a) 24 July, (b) 26 July (c) 29 July, (d) 30 July, and (e) 31 July 2006. Unit: K day^{-1} .

Table 2a. Daily mean radiative forcing of dust aerosols at TOA over the Taklimakan region. Unit: W m^{-2}

Date	24 July	26 July	29 July	30 July	31 July	Mean
SW	12.49	15.6	14.93	14.42	13.13	14.11
LW	28.64	28.86	32.73	27.64	33.65	30.30
Net	41.13	44.46	47.66	42.06	46.78	44.41

Table 2b. Same as Table 2a, but for surface. Unit: W m^{-2} .

Date	24 July	26 July	29 July	30 July	31 July	Mean
SW	-49.70	-67.0	-73.53	-67.27	-66.12	-64.72
LW	19.92	23.37	21.93	22.58	26.36	22.83
Net	-29.78	-43.63	-51.60	-44.69	-39.76	-41.89

Although dust aerosols appear to have less effect on LW radiative heating rates (Fig. 8), they do show a warming effect below the dust layers and cooling near the top of the layers. The maximum warming, which occurs near the surface, is typically about 0.5 K day^{-1} . The LW cooling ranges from

Table 2c. Same as Table 2a, but for in atmosphere. Unit: W m^{-2} .

Date	24 July	26 July	29 July	30 July	31 July	Mean
SW	62.19	82.6	88.46	81.69	79.25	78.83
LW	8.72	5.49	10.8	5.06	7.29	7.47
Net	70.91	88.09	99.26	86.75	86.54	86.31

near zero on 24 July to about -1.5 K day^{-1} on 29 July, which partly compensates the large solar radiative heating near the top of the dust layers. The net aerosol heating near the dust layer top is about 1 K day^{-1} on 24 July, $1.5\text{--}2.0 \text{ K day}^{-1}$ on 26 July, 5.5 K day^{-1} on 29 July, 3 K day^{-1} on 30 July, and 1.5 K day^{-1} on 31 July (Fig. 9). The net heating rates due to the dust aerosols are about $0.5\text{--}1.0 \text{ K day}^{-1}$ below and above the dust layers.

Table 2 shows the daily-mean dust aerosol radiation forcing at the TOA and surface and in the atmosphere over the Taklimakan region. Dust aerosols have a warming effect at the TOA in both SW and LW radiation, which are about 14 and 30 W m^{-2} , respectively. The net warming is 44.4 W m^{-2} . The positive solar radiative forcing is due to the elevated absorbing dust aerosol layer above the highly

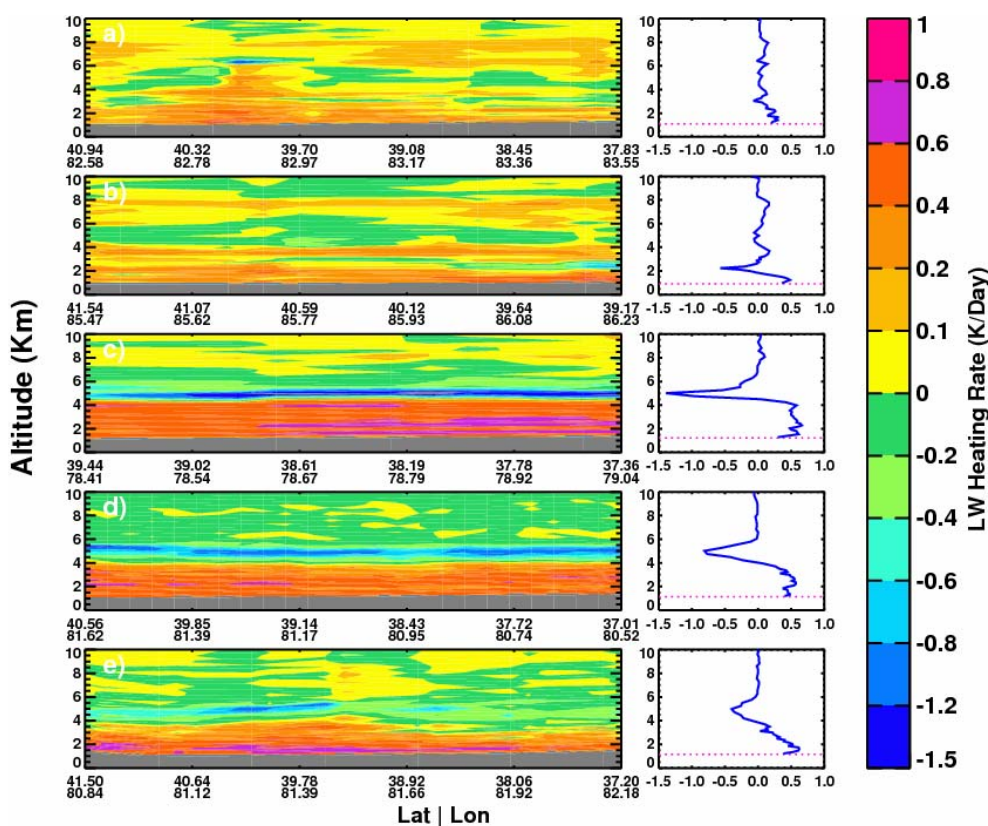


Fig. 8. Same as Fig. 7, but for longwave heating rates.

Table 3. Estimation of uncertainties of radiation forcing. Unit: Wm^{-2} .

	SSA $\pm 6\%$			Surface Albedo $\pm 10\%$			Lidar Ratio $\pm 20\%$		
	TOA	Surface	Atmos	TOA	Surface	Atmos	TOA	Surface	Atmos
SW	∓ 14.815	± 11.450	∓ 26.265	± 4.585	± 3.360	± 1.225	± 1.775	∓ 11.155	± 12.935
LW	∓ 0.360	∓ 0.370	± 0.010	0	0	0	± 4.820	± 3.480	± 1.335
Net	∓ 15.175	± 11.080	∓ 26.255	± 4.585	± 3.360	± 1.225	± 6.595	∓ 7.675	± 14.270

Table 4. Estimation of uncertainties of vertical averaged atmospheric heating rate. Unit: K/day

	SSA $\pm 6\%$	Surface Albedo $\pm 10\%$	Lidar Ratio $\pm 20\%$
SW	∓ 0.272	± 0.010	± 0.138
LW	∓ 0.004	0	± 0.019
Net	∓ 0.276	± 0.010	± 0.157

reflective desert surface. The dust aerosol radiative forcing in the atmosphere is also positive for both SW and LW radiation, which are 78.8 and 7.5 W m^{-2} , respectively, and the total warming is 86.3 W m^{-2} . The dust aerosols cool the

surface significantly by decreasing the incident SW radiation (-64.7 W m^{-2}) but warms it through the dust-emitted LW radiation (22.8 W m^{-2}). The net cooling at the surface is 41.9 W m^{-2} . Table 2 indicates that both SW and LW radiative forcing of dust aerosols play an important role in the radiative energy budget at the TOA and the surface.

6 Uncertainties in radiation forcing

Although this study attempts to minimize the errors by using reliable observations for the model input and to constrain the dust aerosol single-scattering properties, the estimated dust radiative forcing may have some unavoidable uncertainties. They are related to the uncertainties in the CALIPSO

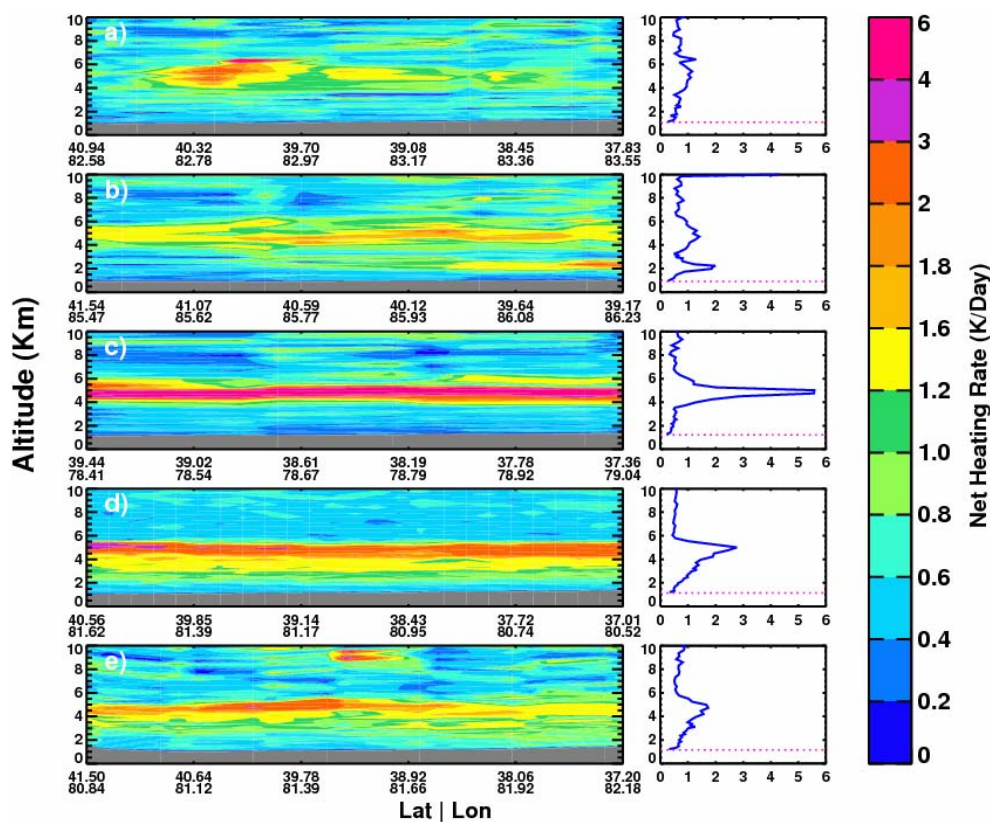


Fig. 9. Same as Fig. 7, but for net heating rates.

lidar ratio for the retrieval of dust aerosol extinction coefficient, surface albedo, and dust aerosol single scattering albedo (SSA). The range of uncertainties in the CALIPSO lidar ratio is about 20% (Winker et al., 2006). The sensitivity test showed that the lidar ratio uncertainty of $\pm 20\%$ can lead to uncertainties of about ± 6.8 , ∓ 7.6 , $\pm 14.4 \text{ Wm}^{-2}$ in the net dust radiative forcing at the TOA, in the atmosphere, and at the surface, respectively (see Table 3). The surface albedo is another possible source of error. If the surface albedo uncertainty is $\pm 10\%$, the dust SW radiation forcing at TOA and surface will be changed about ± 4.6 , $\pm 3.4 \text{ Wm}^{-2}$, respectively (see Table 3). Detailed discussion of uncertainties in SW radiative forcing with respect to surface albedo can be found in the studies of Claquin et al. (1998) and Liao and Seinfeld (1998). The major uncertainty in the estimated dust radiative forcing arises from the SSA. A ± 0.03 uncertainty in the AERONET SSA (Dubovik et al., 2002) can lead to a 12% uncertainty in the SW TOA forcing. Our sensitivity test revealed that the largest error is caused by the SSA uncertainty. The observation study of AERONET shows that maximum dust SW spectral weighted SSA may be 0.94 over Taklimakan, i.e., current value $0.89+6\%$ (Dubovik et al., 2002). Thus, the uncertainty range in the SSA is estimated to be $\pm 6\%$. A $\pm 6\%$ change in SSA (with a constraint that SSA should not be larger than one) can lead to about ∓ 15.2 ,

± 11.1 , $\mp 26.3 \text{ Wm}^{-2}$ uncertainties in the net dust radiative forcing at TOA, in the atmosphere, and at the surface, respectively (see Table 3). Although the aforementioned three parameters have large effects on the estimated dust radiative forcing, the pattern of dust heating rate is not affected. Only the magnitude of the dust heating rate varies with the changes of parameters. The SSA was found to have its largest effect in regulating the magnitude of the dust heating rate. If the SSA increases by 10%, the net vertically averaged atmospheric heating rate will change by roughly 0.27 K day^{-1} (see Table 4). The lidar ratio uncertainty of $\pm 20\%$ can lead to $\sim 0.16 \text{ K day}^{-1}$ uncertainty in the net vertical mean atmospheric heating rate (see Table 4), while 10% changes in the surface albedo can only cause 0.01 K day^{-1} changes in the net vertical mean atmospheric heating rate.

7 Discussion and conclusions

In this study, we investigated the impact of dust aerosols on the radiative energy budget over the Taklimakan Desert during dust episodes in late July 2006. The dust aerosol radiative forcing was estimated using the Fu-Liou model along with CALIPSO and CERES measurements. It was determined that dust aerosols warm the atmosphere over the Taklimakan, especially at the levels between 3 and 6 km where the

maximum aerosol extinction coefficients are found. In the dusty atmospheric layers, the dust typically heats the layer by up to 1–3 K day⁻¹ depending on the dust concentration. The maximum daily mean net (shortwave + longwave) radiative heating rate reached 5.5 K day⁻¹ at 5 km on 29 July. The averaged daily mean net radiative forcings of the dust aerosols, averaged over our case studies, were 44.4, -41.9, and 86.3 W m⁻², respectively, at the TOA, surface, and in the atmosphere. Among these forcings about two thirds of the warming effect at the TOA is due to absorption and emission of longwave radiation by the layer, while about 90% of atmospheric warming is due to absorption of the solar radiation. At the surface, about one third of the dust aerosol solar radiative cooling effect is compensated by the dust aerosol longwave warming effect. This study indicates that both shortwave and longwave radiative forcing of dust aerosols play an important role in the radiative energy budget at the TOA and the surface.

For the radiative effect of the dust aerosol, the most important factors for the shortwave forcing of dust aerosols at the TOA are the aerosol optical depth and the single scattering albedo while the longwave forcing is highly dependent on the vertical profile of the dust aerosols. Previous spectral, simultaneous remote and in situ observations suggest that the single scattering albedo of pure dust at a wavelength of 0.67 μm is predominantly in the range from 0.90 to 0.99, with a central global estimate of 0.96 (Forster, et al., 2007). This is in accordance with the bottom-up modeling of ω based on the hematite content in desert dust sources (Claquin et al., 1999; Shi et al., 2005). Analyses of ω from long-term AERONET sites influenced by Saharan dust suggest an average value of 0.95 at 0.67 μm (Dubovik et al., 2002), while unpolluted Asian dust during the Aeolian Dust Experiment on Climate (ADEC) had an average value of 0.93 at 0.67 μm (Mikami et al., 2006). These high ω values suggest that a significant positive shortwave radiative forcing by dust is unlikely (Forster et al., 2007). However, our results suggest that the single scattering albedo of Taklimakan dust aerosols is about 0.89 at 0.67 μm which is about 6% less than Saharan dust. The mean shortwave radiative forcing at TOA is as much as 14.1 W m⁻².

Acknowledgements. This research is supported by the National Science Foundation of China under grant (40628005, and 40633017) and National Basic Research Program of China (2006CB400501). Q. Fu is also supported by NASA Grant NNX08AF66G. This research was also supported by the CALIPSO and CloudSat projects. The CALIPSO and CERES data were obtained from the NASA Earth Observing System Data and Information System, Distributed Active Archive Center (DAAC) at the Langley Research Center.

Edited by: J. Quaas

References

- Ackerman A. S., Toon, O. B., Stevens, D. E., Heymsfield, A. J., Ramanathan, V., and Welton, E. J.: Reduction of tropical cloudiness by soot, *Science*, 288, 1042–1047, 2000.
- Albrecht, B. A.: Aerosols, cloud microphysics, and fractional cloudiness, *Science*, 245, 1227–1230, 1989.
- Carlson, T. N., and Benjamin, S. G.: Radiative heating rates for Saharan dust, *J. Atmos. Sci.*, 37, 193–213, 1980.
- Claquin, T., Schulz, M., Balkanski, Y. J., and Boucher, O.: Uncertainties in assessing radiative forcing by mineral dust, *Tellus B*, 50, 491–505, 1998.
- Claquin, T., Schulz, M., and Balkanski, Y.: Modeling the mineralogy of atmospheric dust, *J. Geophys. Res.*, 104(D18), 22243–22256, 1999.
- Dubovik, O., Holben, B., Eck, T. F., et al.: Variability of absorption and optical properties of key aerosol types observed in worldwide locations, *J. Atmos. Sci.*, 59, 590–608, 2002.
- Forster, P., Ramaswamy, V., Artaxo, P., Berntsen, T., Betts, R., Fahey, D. W., Haywood, J., Lean, J., Lowe, D.C., Myhre, G., Nganga, J., Prinn, R., Raga, G., Schulz, M., and Van Dorland, R.: Changes in Atmospheric Constituents and in Radiative Forcing, in: *Climate Change 2007: The Physical Science Basis. Contribution of Working Group I to the Fourth Assessment Report of the Intergovernmental Panel on Climate Change*, edited by: Solomon, S., Qin, D., Manning, M., Chen, Z., Marquis, M., Averyt, K. B., Tignor, M., and Miller, H. L., Cambridge University Press, Cambridge, UK and New York, NY, USA, 2007.
- Fu, Q., and Liou, K.-N.: On the correlated k-distribution method for radiative transfer in nonhomogenous atmospheres, *J. Atmos. Sci.*, 49, 2139–2156, 1992.
- Fu, Q., and Liou, K. N.: Parameterization of the radiative properties of cirrus clouds, *J. Atmos. Sci.*, 50, 2008–2025, 1993.
- Hess, M. P., Koepke, P., and Schultz, I.: Optical properties of aerosol and clouds: The software package OPAC, *B. Am. Meteor. Soc.*, 79, 831–844, 1998.
- Huang, J., Lin, B., Minnis, P., Wang, T., Wang, X., Hu, Y., Yi, Y., and Ayers, J. K.: Satellite-based assessment of possible dust aerosols semidirect effect on cloud water path over East Asia, *Geophys. Res. Lett.*, 33, L19802, doi:10.1029/2006GL026561, 2006.
- Huang, J., Minnis, P., Yi, Y., Tang, Q., Wang, X., Hu, Y., Liu, Z., Ayers, K., Trepte, C., and Winker, D.: Summer dust aerosols detected from CALIPSO over the Tibetan Plateau, *Geophys. Res. Lett.*, 34, L18805, doi:10.1029/2007GL029938, 2007.
- Huang, J., Minnis, P., Chen, B., Huang, Z., Liu, Z., Zhao, Q., Yi, Y., and Ayers, J.: Long-range transport and vertical structure of Asian dust from CALIPSO an surface measurements during PACDEX, *J. Geophys. Res.*, 113, D23212, doi:10.1029/2008JD010620, 2008.
- Hu, Y., Liu, Z., Winker, D., Vaughan, M., Noel, V., Bissonnette, L., Roy, G., and McGill, M.: A simple relation between depolarization and multiple scattering of water clouds and its application for lidar calibration, *Opt. Lett.*, 31, 1809–1811, 2006.
- Hu, Y., Vaughan, M., Liu, Z., Lin, B., et al.: The depolarization-attenuated backscatter relation: CALIPSO lidar measurements vs. theory, *Opt. Express*, 15, 5327–5332, 2007.
- Iwasaka, Y., Minoura, H., and Nagaya, K.: The transport and spatial scale of Asian dust-storm clouds: A case study of the dust-storm event of April 1979, *Tellus B*, 35, 189–196, 1983.

- Kato, S., Charlock, T. P., and Rose, F. G.: Paper Computation of Domain-Averaged Irradiance Using Satellite-Derived Cloud Properties, *J. Atmos. Ocean. Technol.*, 22b, 146–164, 2005.
- Koren, I., Kaufman, Y. J., Remer, L. A., and Marins, J. V.: Measurement of the Effect of amazon smoke on inhibition of cloud formation, *Science*, 303, 1342–1345, 2004.
- Kratz, D. P. and Rose, F. G.: Accounting for molecular absorption within the spectral range of the CERES window channel, *J. Quant. Spectrosc. Radiat. T.*, 48, 83, 1999.
- Kruger, O. and Graßl, H.: Albedo reduction by absorbing aerosols over China, *Geophys. Res. Lett.*, 31, L02108, doi:10.1029/2003GL019111, 2004.
- Liao, H. and Seinfeld, J. H.: Radiative forcing by mineral dust aerosols: Sensitivity to key variables, *J. Geophys. Res.*, 103(D24), 31637–31645, 1998.
- Liu, Z., Vaughan, M. A., Winker, D. M., Hostetler, C. A., Poole, L. R., Hlavka, D., Hart, W., and McGill, M.: Use of probability distribution functions for discriminating between cloud and aerosol in lidar backscatter data, *J. Geophys. Res.*, 109, D15202, doi:10.1029/2004JD004732, 2004.
- Liu, Z., Liu, D., Huang, J., Vaughan, M., Uno, I., Sugimoto, N., Kitaka, C., Trepte, C., Wang, Z., Hostetler, C., and Winker, D.: Airborne dust distributions over the Tibetan Plateau and surrounding areas derived from the first year of CALIPSO lidar observations, *Atmos. Chem. Phys.*, 8, 5045–5060, 2008.
- Meloni, D., Sarra, A. D., Iotio, T. D., and Fiocco, G.: Influence of the vertical profile of Saharan dust on the visible direct radiative forcing, *J. Quant. Spectrosc. Radiat. T.*, 93, 497–413, 2005.
- Mikami, M., Shi, G. Y., Uno, I., et al.: Aeolian dust experiment on climate impact: an overview of Japan-China Joint Project ADEC, *Global Planet Change*, 52, 142–172, doi:10.1016/j.gloplacha.2006.03.001, 2006.
- Minnis, P., Trepte, Q. Z., Sun-Mack, S., Chen, Y., et al.: Cloud detection in non-polar regions for CERES using TRMM VIRS and Terra and Aqua MODIS data, *IEEE Trans. Geosci. Remote Sens.*, 46, 3857–3884, 2008.
- Murayama, T., Sugimoto, N., Uno, I., et al.: Ground-based network observation of Asian dust events of April 1998 in east Asia, *J. Geophys. Res.*, 106(D16), 18345–18360, 2001.
- Omar, A., Winker, D., and Won, J.: Aerosol models for the CALIPSO lidar inversion algorithms, *Laser Radar Technology for Remote Sensing*, Proc. SPIE, 5240, 153–164, 2004.
- Rose, F. G. and Charlock, T. P.: New Fu-Liou Code Tested with ARM Raman Lidar and CERES in pre-CALIPSO Exercise, Extended abstract for 11th Conference on Atmospheric Radiation (AMS), Ogden, Utah, USA, 3–7 June 2002, 2002.
- Satheesh, S. K., Vinoj, V., and Moorthy, K. K.: Vertical distribution of aerosols over an urban continental site in India inferred using a micro pulse lidar, *Geophys. Res. Lett.*, 33, L20816, doi:10.1029/2006GL027729, 2006.
- Shi, G. Y., Wang, H., Wang, B., et al.: Sensitivity experiments on the effects of optical properties of dust aerosols on their radiative forcing under clear sky condition, *J. Meteorol. Soc. Japan*, 83A, 333–346, 2005.
- Slingo, A., Ackerman, T. P., Allan, R. P., et al.: Observations of the impact of a major Saharan dust storm on atmospheric radiation balance, *Geophys. Res. Lett.*, 33, L24817 doi:10.1029/2006GL027869, 2006.
- Sokolik, I. N. and Toon, O. B.: Incorporation of mineralogical composition into models of the radiative properties of mineral aerosol from UV to IR wavelengths, *J. Geophys. Res.*, 104, 9423–9444, 1999.
- Stephens, G. L., Vane, D. G., Boain, R. J., Mace, G. G., et al.: The CloudSat Mission and the A-Train: A New Dimension of Space-Based Observations of Clouds and Precipitation, *B. Am. Meteor. Soc.*, 83, 1771–1790, 2002.
- Sun, J., Zhang, M., and Liu, T.: Spatial and temporal characteristics of dust storms in China and its surrounding regions, 1960–1999: Relations to source area and climate, *J. Geophys. Res.*, 106, 10325–10333, 2001.
- Tegen, I., Lacis, A. A., and Fung, I.: The influence on climate forcing of mineral aerosols from disturbed soils, *Nature*, 380, 419–421, doi:10.1038/38041900, 1996.
- Tegen, I., Werner, M., Harrison, S. P., and Kohfeld, K. E.: Relative importance of climate and land use in determining present and future global soil dust emission, *Geophys. Res. Lett.*, 31, L05105, doi:10.1029/2003GL019216, 2004.
- Twomey, S.: The influence of pollution on the shortwave albedo of clouds, *J. Atmos. Sci.*, 34, 1149–1152, 1977.
- Uno, I., Yumimoto, K., Shimizu, A., Hara, Y., Sugimoto, N., Wang, Z., Liu, Z., and Winker D. M.: 3D structure of Asian dust transport revealed by CALIPSO lidar and a 4DVAR dust model, *Geophys. Res. Lett.*, 35, L06803, doi:10.1029/2007GL032329, 2008.
- Uno, I., Amano, H., Emori, S., Kinoshita, K., Matsui, I., and Sugimoto, N.: Trans-Pacific yellow sand transport observed in April 1998: A numerical simulation, *J. Geophys. Res.*, 106(D16), 18331–18344, doi:10.1029/2000JD900748, 2001.
- Wang, S., Wang, J., Zhou, Z., and Shang, K.: Regional characteristics of three kinds of dust storm events in China, *Atmos. Environ.*, 39, 509–520, 2005.
- Wielicki, B. A., Barkstrom, B. R., Harrison, E. F., et al.: Clouds and the Earth's Radiant Energy System (CERES): an earthobserving system experiment, *B. Am. Meteor. Soc.*, 77, 853–868, 1996.
- Winker, D., Vaughan, M., and Hunt, W.: The CALIPSO mission and initial results from CALIOP, *Proc. SPIE*, 6409, 640902, doi:10.1117/12.698003, 2006.
- Zhang, J. L. and Christopher, S. A.: Longwave radiative forcing of Saharan dust aerosols estimated from MODIS, MISR, CERES observations on Terra, *Geophys. Res. Lett.*, 30, doi:10.1029/2003GL018479, 2003.
- Zhang, X. Y., Arimoto, R., and An, Z. S.: Dust emission from Chinese desert sources linked to variations in atmospheric circulation, *J. Geophys. Res.*, 102(D23), 28041–28044, 1997.
- Zhu, A., Ramanathan, V., Li, F., and Kim, D.: Dust plumes over the Pacific, Indian, and Atlantic oceans: Climatology and radiative impact, *J. Geophys. Res.*, 112, D16208, doi:10.1029/2007JD008427, 2007.